Effectiveness of Symbol-Rate Optimization with PM-16QAM Subcarriers in WDM Transmission

F. P. Guiomar[(1)], A. Carena[(1)], G. Bosco[(1)], L. Bertignono[(1)], A. Nespola[(2)] and P. Poggiolini[(1)]

[(1)] *DET, Politecnico di Torino, Corso Duca degli Abruzzi, 24, 10129, Torino, Italy, fernando.guiomar@polito.it*
[(2)] *Istituto Superiore Mario Boella, via Pier Carlo Boggio 61, 10138 Torino, Italy, nespola@ismb.it*

Abstract: We demonstrate up to 9% reach gain provided by symbol-rate optimization (SRO) with PM-16QAM subcarriers in WDM transmission. Applying an ideal CPE, we also discuss on the potentially achievable SRO gains enabled by enhanced phase noise compensation.

OCIS codes: (060.2360) Fiber optics links and subsystems; (060.1660) Coherent communications.

1. Introduction

Several analytical, simulation and experimental papers have recently reported on the existence of an optimum symbol-rate that minimizes the nonlinear interference (NLI) noise generated along signal propagation in dispersion unmanaged optical links [1–4]. This so-called symbol-rate optimization (SRO) effect has been experimentally observed using PM-QPSK modulated subcarriers in WDM transmission, enabling up to 11% extended reach [1]. Very recently, a massively wideband (C+L bands) experiment has confirmed the relevance of SRO with PM-QPSK subcarriers (up to 0.8 dB gain in Q-factor), whereas a more modest improvement was found with PM-16QAM (0.2 dB) [2]. Other single-channel transmission experiments employing PM-16QAM subcarriers have shown reach gains up to 14% [3, 4].

The impact of the modulation format on NLI generation has been analytically assessed [5, 6] and experimentally demonstrated [7]. Being more Gaussian-like, higher-order QAM formats were found to suffer from enhanced NLI generation, which may reduce the potential gains achievable through SRO. However, it has been recently suggested that most of the added NLI associated with higher-order QAM is actually generated in the form of long-correlated nonlinear phase noise (NLPN) [8]. Mitigating NLPN in such systems may then be the decisive factor to unlock the full potential of SRO under highly spectral efficient transmission.

In this paper we provide a comprehensive analytical, simulative and experimental analysis of a long-haul optical link composed of 31 channels modulated as PM-16QAM multi-subcarrier (MSC) signals, with symbol-rate varying from 24 down to 2 GBaud. Exploring a data-aided implementation of carrier-phase estimation (CPE), we assess the impact of NLPN in our system and the respective increased potential benefit coming from its enhanced mitigation.

2. Experimental setup

The experimental setup is shown in Fig. 1a. At the transmitter side, 31 channels are generated each at an aggregate symbol-rate of 24 GBaud with an inter-channel separation of 28 GHz. Through digital subcarrier multiplexing, each channel is then transmitted either as 1×24 GBaud, 2×12 GBaud, 4×6 GBaud, 6×4 GBaud, 8×3 GBaud or 12×2 GBaud, with an inter-subcarrier spacing of 1.05× subcarrier symbol-rate. All subcarriers are shaped by a root-raised-cosine filter with roll-off 0.05. Uncorrelated PRBS data is assigned to each subcarrier tributary, with length varying between 2^{15} (highest symbol-rate) and 2^{11} (lowest symbol-rate) symbols. Digital pre-emphasis is applied to compensate for the bandwidth limitation of the digital-to-analog converter (DAC) operating at 64 GSa/s. The channel under test (CUT) is generated by an external cavity laser (ECL) with <100 kHz linewidth and modulated in a dual-polarization Mach-Zehnder modulator (MZM), while the remaining 30 interfering channels are generated by distributed-feedback (DFB) lasers and modulated (separately for even and odd channels) by a single-polarization MZM followed by a polarization multiplexing emulator (PME).

The recirculating loop is composed of 4 spans of pure silica core fiber (PSCF) with average length of 108 km, dispersion parameter of 20.12 ps/(nm·km) and attenuation coefficient of 0.162 dB/km. The total span loss, including all insertion losses, is 18.75 dB. We use EDFA-only amplification (noise figure of 5.2 dB) and a spectrally-resolved gain equalizer (GEQ) to compensate for the EDFA gain-tilt and ripples. Finally, a loop synchronized polarization scrambler is used to statistically average the polarization effects.

At the receiver, the CUT is filtered by a tunable optical filter (TOF) and mixed with an ECL (<100 kHz). The coherently detected signal is sampled by a 50 GSa/s real-time oscilloscope (Tektronix DPO73304DX). Digital signal

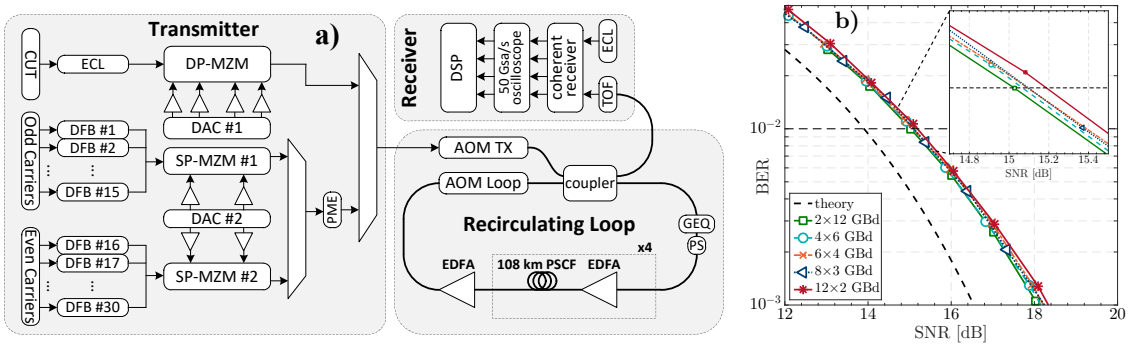

Fig. 1: a) laboratorial setup for MSC transmission; b) B2B performance.

processing of the received MSC signal starts with front-end correction, followed by chromatic dispersion compensation over the entire MSC signal, whose subcarriers are then demultiplexed and converted to baseband. Frequency offset removal is applied by a sliding-window spectral method, followed by a first coarse carrier phase estimation (CPE) applied over one of the central subcarriers, using the 16QAM-modified (QPSK partitioning) V&V algorithm.The estimated phase noise is then removed from all subcarriers, allowing for the compensation of the transmitter IQ skew with a 51-tap least mean squares (LMS)-driven 8×8 real-valued equalizer, initialized in data-aided mode for tap convergence and then switched to decision-directed mode. After downsampling to 1 SpS, a second V&V CPE stage is applied independently over each subcarrier with an optimized block length. Finally, the signal is decoded and the BER per subcarrier is counted. The system performance is measured in terms of the average BER among all subcarriers.

The B2B performance of the different MSC configurations is shown in Fig. 1b. The system operates with a B2B penalty of ∼1.1 dB relatively to the theoretical limit, which is kept within 0.1 dB of deviation for all MSC configurations, except for the 12×2 GBaud case, which was found to suffer from ∼0.2 dB extra penalty.

3. Experimental results

In order to assess the issue of NLI modulation format dependence, in this work we have considered two distinct EGN analyses: i) EGN-16QAM: analytical NLI prediction for the actual experimental scenario condition, i.e., all subcarriers modulated as PM-16QAM; ii) EGN-QPSK: analytical NLI prediction hypothetically assuming that all subcarriers were actually modulated as PM-QPSK, following the insights of [8], which suggest the modulation format independence of NLI when NLPN is fully suppressed. In addition, we also consider two distinct CPE methods for the processing of simulation and experimental results: i) a realistic blind CPE with optimized block length; ii) an ideal data-aided CPE, controlled to maximize the "circularity" of the PM-16QAM constellation points.

The maximum reach achieved by each MSC configuration employing the realistic blind CPE is shown in Fig. 2a, where the experimental results are directly compared against EGN model predictions and split-step-based simulations using the commercial software OptSim. The obtained results reveal an excellent agreement between the experimental, simulation and EGN-16QAM results, yielding a peak gain of ∼9% in maximum reach for the 8×3 GBaud configuration, relatively to the baseline 1×24 GBaud. The good agreement between experimental/simulation results and the EGN-16QAM confirms the modulation-format dependence of NLI and suggests that the applied CPE has limited NLPN compensation capability, as it will become apparent from our subsequent analysis.

Indeed, even after optimizing the CPE block length, we observed that the PM-16QAM constellation symbols were still polluted with non-negligible phase noise, as can be observed in the inset of Fig. 2d. In order to try to remove this excess phase noise, we have considered an alternative ideal V&V CPE, operating in fully data-aided mode. Similarly to the work of [9], we have adopted a figure of merit (FOM) for the signal "circularity" that is defined as the ratio between the variance of the phase and amplitude noise components of the constellation points. A PM-16QAM constellation with perfectly "circular" points is then characterized by FOM $= 1$. With the ideal data-aided CPE approach we aim at reaching FOM ≈ 1, by optimizing the CPE data block length. Note that in this process the variance of the amplitude noise component is left untouched.

In Figs. 2d and 2e we assess the FOM after realistic and ideal CPE, for the case of 8×3 GBaud after 28 spans, at the optimum launch power. With the realistic CPE, the optimum BER performance is found at a large block length of 200 taps, where FOM > 1.3. With the ideal CPE, a block length of 8 taps achieves FOM ≈ 1. This suggests that NLPN correlation is only a few samples, when transmitting at 3 GBaud, so that the optimal block length should be short. However, the realistic CPE cannot use such short block length since it requires a sufficiently large number of samples

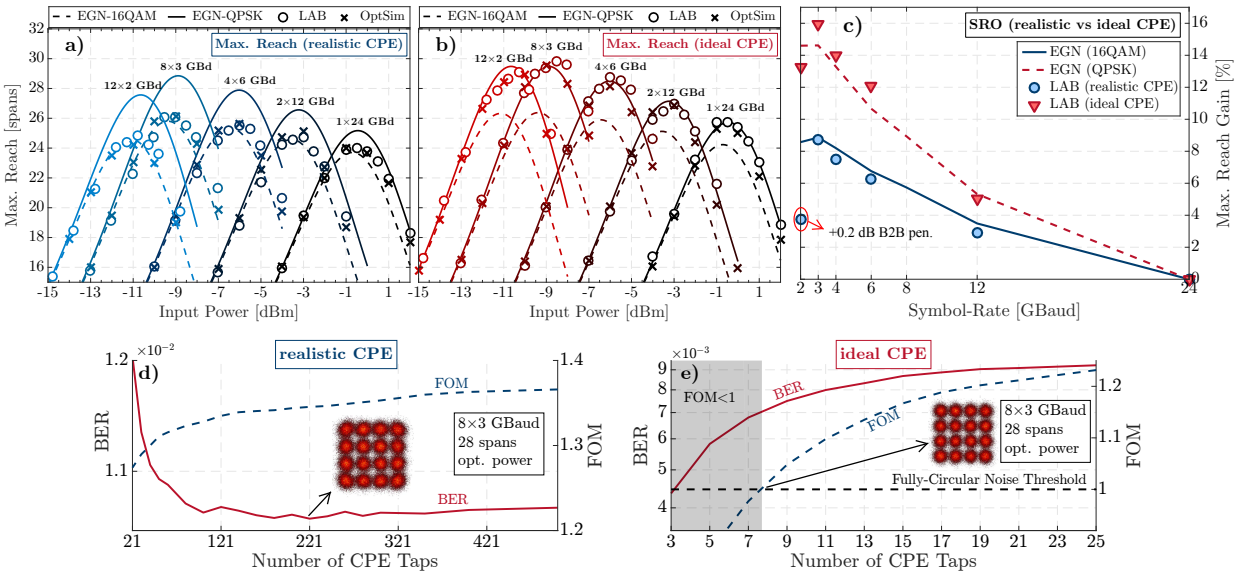

Fig. 2: Experimental results. a) and b) Maximum reach vs input power applying realistic (a) and ideal (b) CPE (for ease of visualization, 6×4 GBaud results are not shown); c) maximum reach gain obtained through SRO; d) CPE block length optimization applying realistic (a) and ideal (b) CPE.

to average out the effect of uncorrelated additive noise on phase estimation. This result highlights the difficulty of compensating for NLPN using standard CPE in multi-subcarrier systems operating at a low Baud rate.

The same procedure has been repeated for all MSC configurations, transmitted powers and propagation distances. The resulting maximum reach employing the ideal CPE, at block length such that FOM ≈ 1, is shown in Fig. 2b. As previously suggested in [8], we observe that the system performance after ideal CPE becomes very well described by the EGN-QPSK analytical prediction (note though that in [8] a different ideal CPE was used, the "PN receiver"). When using the ideal CPE, not only the absolute maximum reach is increased, but also the SRO effect is enhanced, yielding a maximum reach gain over the baseline 1×24 GBaud scenario of more than 15%, as shown in Fig. 2c. It is worth mentioning that the B2B performance with the ideal CPE has been slightly improved by 0.1 dB, now yielding a constant B2B penalty of 1 dB for all MSC configurations. This has been taken into account in the EGN and OptSim results of Fig. 2b. Also note that varying the B2B penalty alone was not found to have any visible impact on SRO.

The ideal CPE clearly cannot be realized. On the other hand, we think that it provides a rough estimate of the potential improvement in performance that could be reached if NLPN could be eliminated in multi-subcarrier systems, as effectively as it is typically eliminated in single-carrier high-baud-rate systems. This may be possible if CPE specifically optimized for MSC transmission were designed, which is the subject of our ongoing research.

4. Conclusions

Employing realistic blind CPE, we have demonstrated up to 9% extended reach enabled by subcarrier-based WDM transmission, relatively to a baseline symbol-rate of 24 GBaud. The results are in good agreement with the analytical EGN-16QAM predictions, highlighting the reduced capability of standard CPE to remove NLPN in such systems. The results obtained with an ideal CPE approach also indicate that important gains in terms of reach and SRO effectiveness could be potentially achieved by enhanced NLPN mitigation methods.

This work was partially supported by the European Commission through a Marie Sklodowska-Curie individual fellowship, project Flex-ON (653412), and by the Cisco University Research Program Fund, a corporate advised fund of Silicon Valley Community Foundation. We thank Synopsys Inc. for supplying the OptSim simulator.

References

[1] P. Poggiolini *et al*, "Analytical and Experimental Results on System Maximum Reach ...," *JLT*, vol. 34, no. 8, pp. 1872–1885, 2016.
[2] J. -X. Cai *et al*, "Experimental Study of Subcarrier Multiplexing Benefit in 74 nm ...," *ECOC*, pp. 677–679, 2016.
[3] M. Qiu *et al*, "Digital subcarrier multiplexing for fiber nonlinearity mitigation ...", *Opt. Express*, vol. 22, no. 15, pp. 18770–18777, 2014.
[4] F. Buchali *et al*, "Study of electrical subband multiplexing at 54 GHz modulation bandwidth for 16QAM ...", *ECOC*, pp. 49–51, 2016.
[5] R. Dar *et al*, "Properties of nonlinear noise in long, dispersion-uncompensated fiber ...", *Opt. Express*, vol. 21, no. 22, pp. 25685–25699, 2013.
[6] A. Carena *et al*, "EGN model of non-linear fiber propagation", *Opt. Express*, vol. 22, no. 13, pp. 16335–16362, 2014.
[7] L. Galdino *et al*, "Experimental Demonstration of Modulation-Dependent Nonlinear Interference ...", *ECOC*, pp. 950–952, 2016.
[8] A. Nespola *et al*, "Independence of the Impact of Inter-Channel Non-Linear Effects on Modulation Format ...", *ECOC*, pp. 485–487, 2016.
[9] C. Schmidt-Langhorst *et al*, "Experimental analysis of nonlinear interference noise ...", *ECOC*, paper ID: 0666, 2015.